Dielectric hysteresis loops of first-order ferroelectric bilayers and antiferroelectrics

Lye-Hock Ong, Junaidah Osman, and D. R. Tilley
School of Physics, Universiti Sains Malaysia, 11800USM Penang, Malaysia
(Received 25 June 2001; published 19 March 2002)

We consider a ferroelectric bilayer or superlattice with an antiferroelectric interface coupling between two materials which have first-order phase transitions in the bulk. The system is described by a Landau free-energy expression including a bilinear coupling. A detailed discussion is given for the case when the component materials are the same. For equal thicknesses the free energy is the same as for a bulk first-order antiferroelectric. For this, analytical expressions are given for the supercooling, thermodynamic and superheating critical temperatures. Dielectric hysteresis loops are calculated numerically, and it is shown that they can be classified according to a simple scheme. A qualitative discussion is given of the effect of including biquadratic interface coupling. For a general thickness ratio in the bilayer, an analytical result is found for the supercooling temperature and the other two are calculated numerically. Typical dielectric hysteresis loops are shown, and a classification scheme is presented.

DOI: 10.1103/PhysRevB.65.134108 PACS number(s): 77.80.Dj

I. INTRODUCTION

Ferroelectrics, as it is recalled, have simple hysteresis loops,[1–5] whereas the hysteresis for an antiferroelectric material consists of double loops. In a recent paper[6] we pointed out that if a bilayer of two ferroelectrics can be produced with antiferroelectric coupling across the interface, then a wide range of dielectric hysteresis loops is possible, going from basically antiferroelectric for $L_1 \approx L_2$ to basically ferroelectric for $L_1 \gg L_2$, where L_1 and L_2 are the thicknesses of the component layers. The kind of system we have in mind is a physical trilayer $A/B/A'$, in which a thin layer of a ferroelectric B is interposed between ferroelectric layers A and A'. The basic assumption that was made in Ref. 6, and which we continue to make here, is that layer B produces an antiferroelectric coupling between ferroelectric layers A and A'. In modeling this system, we replace B by an effective coupling JP_1P_2 between the ferroelectric polarizations in A and A', so that we may represent the system as an effective bilayer $A//A'$. A magnetic analog is the Fe/Cr/Fe trilayer, in which it is well known[7] that in a suitable thickness range the Cr layer produces an antiferromagnetic coupling between the Fe layers. This system is often modeled by a ''bilayer'' Fe//Fe, with the Cr layer replaced by an effective exchange between the Fe layers.

To simplify the analysis, we assumed that the layers were made of materials in which the transition to ferroelectricity is second order. However, since most ferroelectric phase transitions are first order, it is worthwhile to extend the analysis to first-order materials, and that is the purpose of this paper. As before, we describe the bilayer by a Landau-Devonshire free-energy expression. The key term in this is a coupling JP_1P_2 across the interface, and it is analogous to the magnetic coupling in giant magnetoresistance[7] where the value of J depends on the material used to serve as the coupling mechanism between the interfaces. This expression is symmetry allowed, and should therefore be included; furthermore it appears in a continuum approximation to the Ising-model in transverse field (IMTF) Hamiltonian for a bilayer.[8] The IMTF analysis leads to higher-order coupling terms like $J_2P_1^2P_2^2$, which is also symmetry allowed. We do not give a detailed analysis of the effect of including this term but we do give a brief qualitative discussion.

The free-energy expression is presented in Sec. II, and rewritten in dimensionless units. In order to make the analysis tractable we assume, as before,[6] that the materials of the individual layers are identical, $A=A'$. As discussed above, we replace $A/B/A$ by $A//A$ with B represented by the exchange-like final term in our Eq. (1). For $L_1=L_2$ the free energy is the same as that for a first-order antiferroelectric and for this special case a number of analytical results can be derived. We devote Sec. III to a discussion of this case for two reasons. First the antiferroelectric is of interest in itself, and the available discussions are no more than outlines.[3–5] Second, the results in this special case are very helpful in giving a clear account of the results for general L_1/L_2, which are the subject of Sec. IV. For both special and general cases we start by finding the critical temperatures (supercooling t_{SC}, thermodynamic t_C, and superheating t_{SH}) in a zero applied field E; some of the results are analytical and some are numerical. We then numerically explore the minimum points of the free energy in the P_1-P_2 plane for nonzero E, and use these to draw dielectric hysteresis loops. It will be seen that a wide variety of loops is possible, but a simple generalization is that the form of a loop is characteristic of the range $t_{SC}<t<t_C$ in which the temperature t lies. Some conclusions are presented in Sec. V.

II. FREE ENERGY

Our analysis is based on the free-energy expression

$$\frac{F}{S}=\frac{A_1}{2\varepsilon_0}P_1^2L_1+\frac{B_1}{4\varepsilon_0^2}P_1^4L_1+\frac{C_1}{6\varepsilon_0^3}P_1^6L_1-EP_1L_1+\frac{A_2}{2\varepsilon_0}P_2^2L_2+\frac{B_2}{4\varepsilon_0^2}P_2^4L_2+\frac{C_2}{6\varepsilon_0^3}P_2^6L_2-EP_2L_2+JP_1P_2, \quad (1)$$

where S is the surface area of the sample; L_1 and L_2 are the thicknesses of the layers, A_i, B_i, and C_i, $i=1,2$ are the

Landau coefficients; E is the applied static field; and J is the assumed coupling interaction. A_i is as usual assumed to be temperature dependent, $A_i=\alpha_i\,(T-T_{i0})$ where α_i is the inverse Curie constant, and T_{i0} the critical supercooling temperature of layer i. B_i and C_i are assumed to be temperature independent and for first-order transitions $B_i<0$ and $C_i>0$. The first three terms in Eq. (1) apply to layer 1, and are the standard free energy for a first-order bulk ferroelectric; the fourth term describes coupling of layer 1 to the field. The next four terms are the same thing for layer 2, and the final term is the interface coupling. We assume $J>0$ so that the coupling favors antiferroelectric ordering $P_1P_2<0$. A ferroelectric coupling $J<0$ might also occur, but is unlikely to be of great interest since its basic effect would be to make the bilayer similar to a single ferroelectric layer. As mentioned previously,[6] we omit a possible variation of P with distance across each film. This allows us to concentrate on the qualitative effects of the coupling term; a numerical scheme is available[7] that would allow the inclusion of spatial variation of P.

If materials 1 and 2 are different, the variety of equilibrium states and dielectric hysteresis loops described by (1) is very large. In order to concentrate on the effects produced by the interface coupling we therefore, as before,[6] assume that materials 1 and 2 are the same, so we write $A_1=A_2=A$, $B_1=B_2=-B$ and $C_1=C_2=C$, where we insert the sign of the B terms explicitly so that B is positive. We now follow the conventional scaling for first-order materials,[3,9] and also introduce a dimensionless length variable l:

$$t=\frac{4\alpha C(T-T_0)}{B^2}, \tag{2}$$

$$p_i=P_i/P_0 \quad \text{with} \quad i=1,2 \quad \text{and} \quad P_0^2=\varepsilon_0 B/(2C), \tag{3}$$

$$l=L_1/(L_1+L_2), \tag{4}$$

and we obtain

$$f=\tfrac{1}{2}t[lp_1^2+(1-l)p_2^2]-\tfrac{1}{2}[lp_1^4+(1-l)p_2^4] +\tfrac{1}{6}[lp_1^6+(1-l)p_2^6]-e[lp_1+(1-l)p_2]+jp_1p_2, \tag{5}$$

where

$$f=\frac{F}{F_0} \quad \text{with} \quad F_0=\frac{SB^3(L_1+L_2)}{8C^2}, \tag{6}$$

$$e=\frac{E}{E_0} \quad \text{with} \quad E_0^2=\frac{B^5}{32\varepsilon_0 C^3}, \tag{7}$$

$$j=\frac{J}{J_0} \quad \text{with} \quad J_0=\frac{B^2(L_1+L_2)}{4\varepsilon_0 C}. \tag{8}$$

The scaling introduced here has the advantage that all first-order materials are described by universal curves, but there is the disadvantage, as seen from Eq. (2), that the value of the dimensionless temperature t corresponding to absolute zero is material dependent. To this extent the scaling is only quasiuniversal. We should mention that previously[6] we used the dimensionless length parameter $l=L_2/L_1$ but the more symmetric definition in Eq. (4) is preferable.

Our subsequent analysis is based on the free energy f given in Eq. (5) and we make the usual assumption that stable (and metastable) states of the bilayer correspond to minima of f with respect to variations of p_1 and p_2. These are given by solutions of the simultaneous equations

$$tlp_1-2lp_1^3+lp_1^5-el+jp_2=0, \tag{9}$$

$$t(1-l)p_2-2(1-l)p_2^3+(1-l)p_2^5-e(1-l)+jp_1=0. \tag{10}$$

Subsequently we plot dielectric hysteresis loops as $lp_1+(1-l)p_2$ versus e.

For the bulk first-order ferroelectric analytical results can be found[3] for $t_{\rm SC}$, t_C, and $t_{\rm SH}$ namely,

$$t_{\rm SC}=0, \quad t_C=0.75, \quad t_{\rm SH}=1.0. \tag{11}$$

In addition, there is a "field-induced ferroelectric phase," that is, a phase with $p\neq 0$ in nonzero field, in a temperature range $t_{\rm SH}<t<t_2$, and the upper temperature limit of this phase is

$$t_2=1.8. \tag{12}$$

For general l the only one of these for which an analytic expression can be found is $t_{\rm SC}$. This is the temperature at which the linearized form of Eqs. (9) and (10) for $e=0$ has a solution, i.e.,

$$t_{\rm SC}=\frac{j}{\sqrt{l(1-l)}}. \tag{13}$$

At first sight the divergence of $t_{\rm SC}$ as $l\to 0$ or $l\to 1$ is puzzling and as will be seen in Sec. IV since $t_{\rm SC}$ is the smallest of the critical temperatures where the others also diverge. The condition from which $t_{\rm SC}$ is calculated is that the paraelectric (PE) phase $p_1=p_2=0$ becomes locally unstable for $e=0$, so that Eq. (13) is the condition for the determinant of the second derivatives of f with respect to p_1 and p_2 to vanish at the origin. This condition involves only the quadratic terms in f, so we are concerned with the behavior near the origin of

$$f_Q=\frac{1}{2}t[lp_1^2+(1-l)p_2^2]+jp_1p_2=f_0+f_C, \tag{14}$$

where $f_C=jp_1p_2$ is the coupling term. This has the form of a saddle point at the origin, with f_C increasing in the two quadrants where p_1 and p_2 have the same sign and decreasing in the quadrants where they have opposite signs. Thus f_C destabilizes the PE phase for paths in these latter quadrants, which is why $t_{\rm SC}$ is larger than the bulk value. The level surfaces of f_0 are ellipses, and for small l these are highly elongated along the p_1 axis. In terms of f_0, therefore, the energy cost of a movement of (p_1,p_2) along a line with p_2 positive and close to the negative p_1 axis is small, so that the

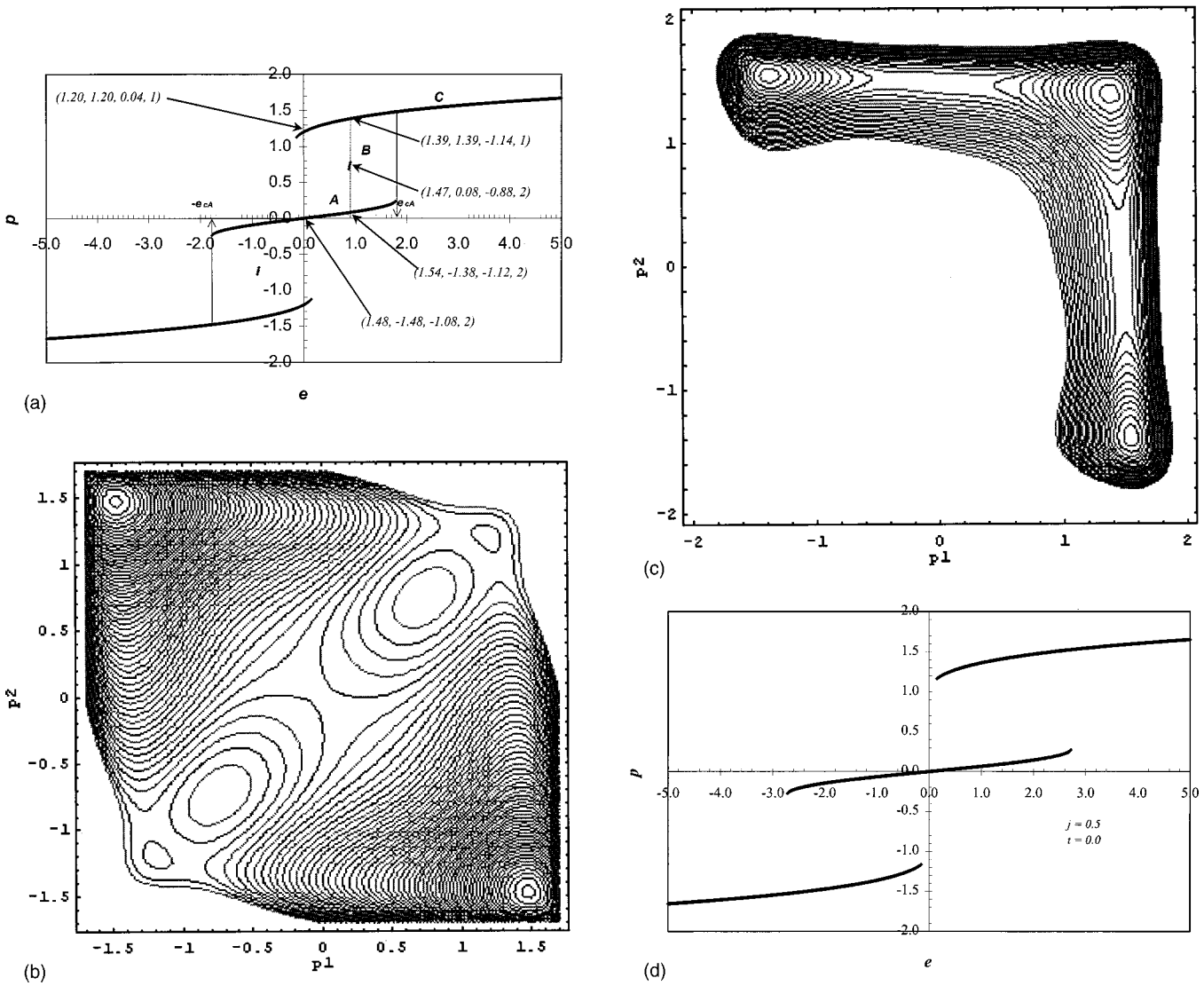

FIG. 1. (a) Dielectric hysteresis loops $p=(p_{1m}+p_{2m})/2$ vs e for equal-layer thicknesses $l=\frac{1}{2}$, coupling $j=0.3$, and temperature $t=0.2$. The annotations in the form (p_1,p_2,f,d) are the locations of minima of f and values of f at minima. These minima correspond to the minimum points in the contour plots in (b) and (c). d is the "degeracy" (1 or 2), because p_1 and p_2 are interchangeable in giving the same value of f. (b) Contour plot of f vs (p_1,p_2) for $e=0$. (c) Contour plot of f vs (p_1,p_2) for $e=0.9$. (d) Dielectric hysteresis loops $p=(p_{1m}+p_{2m})/2$ vs e for equal-layer thicknesses $l=\frac{1}{2}$, coupling $j=0.5$, and temperature $t=0$.

temperature at which the PE phase is destabilized by f_C increases as l decreases. This is the reason for the divergences with l in Eq. (13).

Another way of explaining the divergence of t_{SC} in (13) is to understand the competing effect between t and j in Eq. (14). The effect of j, as mentioned, is to make p_1 and p_2 antiparallel whereas the effect of temperature t is to realign both p_1 and p_2 to a paraelectric phase. Now imagine making layer L_1 thinner with L_2 fixed in thickness, thus depicting the situation where $l\rightarrow 0$. As L_1 gets thinner, the value of p_1 decreases and Eq. (14) approximately becomes $f_Q \cong (1/2)tp_2{}^2+jp_1p_2=f_0+f_C$. Since j and p_2 stay constant, this leads to a decrease in f_C, therefore, in order to maintain the free energy, t has to increase in value thus explaining the reason for its divergence.

III. EQUAL THICKNESSES: THE BULK ANTIFERROELECTRIC

As mentioned, for $l=\frac{1}{2}$ the free energy f in Eq. (5) takes the same form as that for a bulk antiferroelectric, or more precisely $2f$ has the conventional form of the antiferroelectric f_A:

$$2f=f_A=\tfrac{1}{2}t(p_1^2+p_2^2)-\tfrac{1}{2}(p_1^4+p_2^4)+\tfrac{1}{6}(p_1^6+p_2^6)-e(p_1+p_2)+2jp_1p_2. \quad (15)$$

This describes a two-sublattice antiferroelectric with intersublattice coupling $2j$. The critical temperatures can be found from the zero-field expression for f_A. Because of the cou-

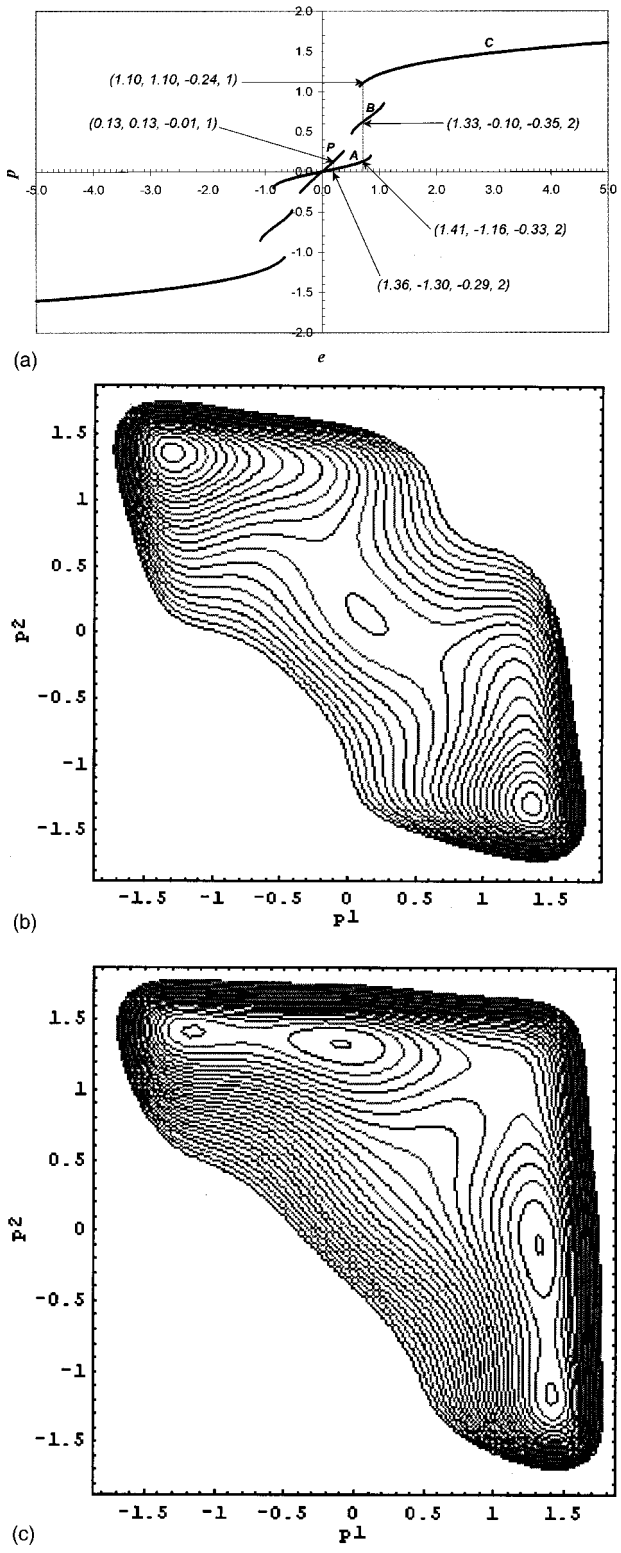

FIG. 2. (a) Dielectric hysteresis loops $p=(p_{1m}+p_{2m})/2$ vs e for equal-layer thicknesses $l=\frac{1}{2}$, coupling $j=0.3$, and temperature $t=1.0$. The annotations in the form (p_1,p_2,f,d) are the locations of minima of f and values of f at minima. These minima correspond to the minimum points in the contour plots in (b) and (c). d is the ''degeracy,'' (1 or 2), because p_1 and p_2 are interchangeable in giving the same value of f. (b) Contour plot of f versus (p_1,p_2) for $e=0.2$. (c) Contour plot of f vs (p_1,p_2) for $e=0.7$.

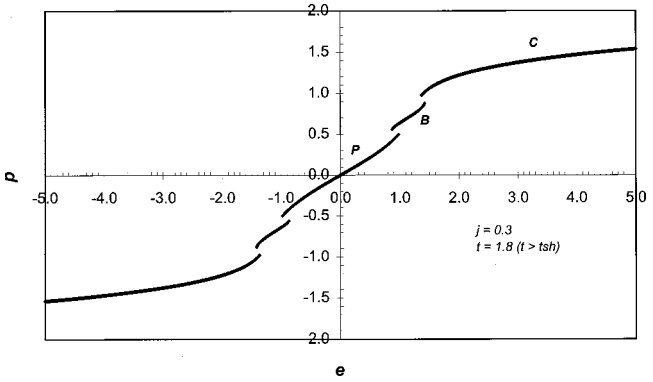

FIG. 3. Dielectric hysteresis loops $p=(p_{1m}+p_{2m})/2$ vs e for equal-layer thicknesses $l=\frac{1}{2}$, coupling $j=0.3$, and temperature $t=1.8$.

pling term the relevant minimum points of f_A satisfy $p_2=-p_1$ so that Eq. (15) becomes

$$f=\tfrac{1}{2}(t-2j)p_1^2-\tfrac{1}{2}p_1^4+\tfrac{1}{6}p_1^6. \tag{16}$$

This is the same as the equivalent equation for a first-order ferroelectric[3] with the replacement $t\rightarrow t-2j$. The same comment applies to Eqs. (9) and (10) for the first derivatives. The critical temperatures can be derived in the same way as those for the ferroelectric. At the supercooling temperature the linearized form of Eq. (9) has a solution, so that $t_{SC}-2j=0$; this is the same as Eq. (13) for $l=\frac{1}{2}$. For $t_{SC}<t<t_{SH}$, there are two local minima of f, and at the thermodynamic critical temperature t_C the values of f at these are equal. At t_{SH} the minimum corresponding to the metastable ordered state disappears, so t_{SH} is given by simultaneous solution of $\partial f/\partial p_1=0$ and $\partial^2 f/\partial p_1^2=0$. Finally, at t_2, the upper temperature

TABLE I. Summary of the behavior of lines in the DHL for $l=0.5$ and $j=0.3$, with t.

t	A line	B line	C line	P line
$t<t_{SC}$	Passes through (0, 0), becomes shorter as t increases	Appears for $e\neq 0$	Crosses $e=0$ only for low values of t.	Does not appear
$t_{SC}<t<t_C$	Passes through (0, 0), becomes shorter as t increases	Becomes longer	Appears at $e\neq 0$	Begin to appear
$t_C<t<t_{SH}$	Passes through (0, 0) disappearing	maintain	Appears at higher e	Becomes longer
$t_{SH}<t<t_2$	disappeared	maintain	Appears at even higher e	Becomes longer

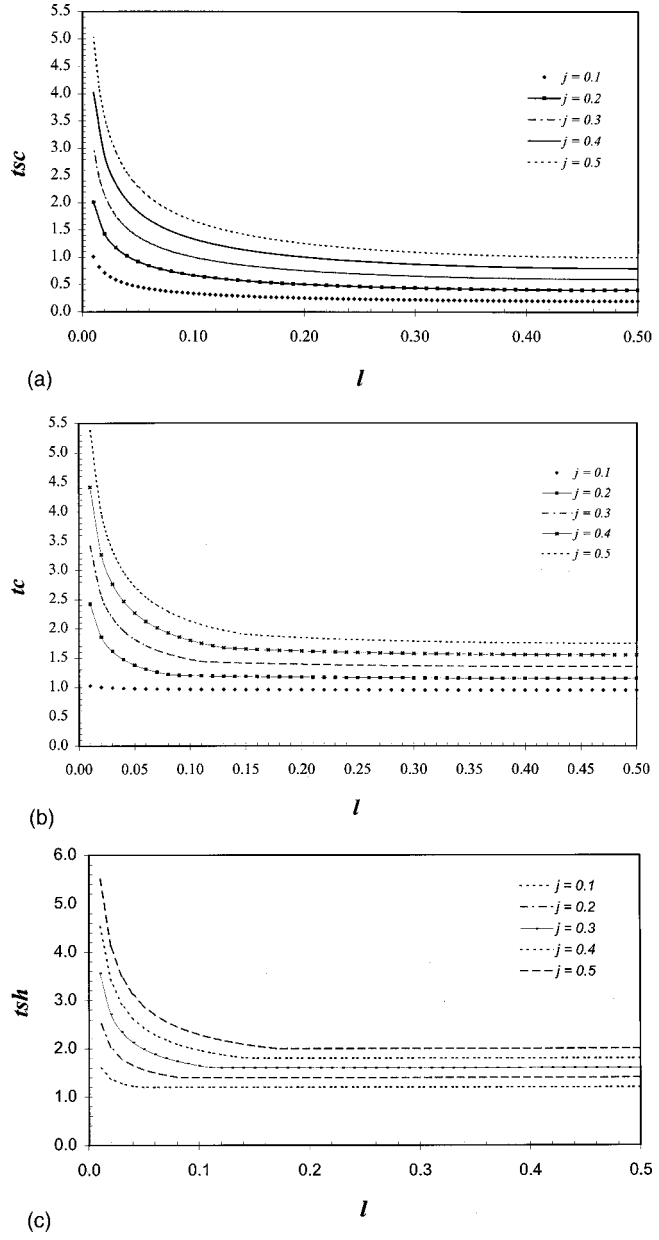

FIG. 4. Dependence on the thickness parameter l of (a) t_{SC}, (b) t_C, and (c) t_{SH}. Values of the coupling constant j are 0.1 (lowest curve on each graph), 0.2, 0.3, 0.4, and 0.5 (highest curve on each graph).

limit of the field-induced ferroelectric state, a non-zero-p_1 point of inflection in f disappears, so t_2 is the highest temperature at which $\partial^2 f/\partial p_1^2=0$ has a solution. In view of the form of Eq. (16), application of these rules shows that for the antiferroelectric the values given in Eqs. (11) and (12) are simply offset by $2j$:

$$t_{\mathrm{SC}}=2j, t_C=0.75+2j, \quad t_{\mathrm{SH}}=1.0+2j, \quad t_2=1.8+2j. \tag{17}$$

Our main emphasis is on the dielectric hysteresis loop (DHL), which is defined as the graph of $p=(p_{1m}+p_{2m})/2$ versus e, where (p_{1m},p_{2m}) is the position of a local minimum of f. Since p is the electric polarization in dimensionless units, the DHL corresponds to measured hysteresis loops.

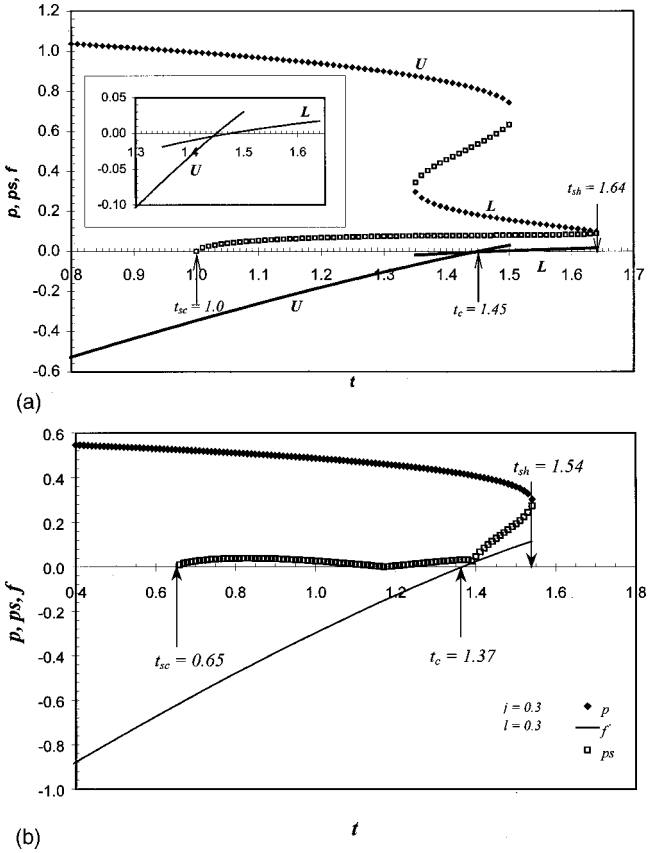

FIG. 5. Temperature dependence of $p=lp_1+(1-l)p_2$ for $j=0.3$ and l equal to (a) 0.1 and (b) 0.3. Points υ are local minima (p) of f and $\square$ are saddle points (p_s). The value of f is plotted as solid line with separate curves in (a) for the upper and lower equilibrium curves U and L. Part of this is shown enlarged in the inset graph.

The values of p_{1m} and p_{2m} are found by numerical solutions of Eqs. (9) and (10). A number of qualitative comments about the possible locations of (p_{1m},p_{2m}) can be made from the free energy expression [Eq. (15)]. We write this as

$$f_A=f_0+f_E+f_C, \tag{18}$$

where f_0 now stands for the first three terms, f_E is the field term, and, as in Eq. (14), f_C is the coupling term. f_0 is the sum of identical terms for the two layers, say $f_0=f_1+f_2$. Since it contains only even terms, the surface describing this term has four-fold symmetry in the (p_1,p_2) plane. For example, for $t_{\mathrm{SC}}<t<t_{\mathrm{SH}}$, where t_{SC} and t_{SH} are the bulk values, f_1 has a local minimum at $p_1=0$ (PE) and another at nonzero values $p_1=\pm p_0$ say (FE). Consequently the f_0 surface has a local minimum at the origin and four more at $(\pm p_0,\pm p_0)$. The coupling term f_C favors antiparallel alignment, $p_2\approx -p_1$. Thus when added to f_0, and in the absence of a field, f_C deepens the FE minima at $(p_0,-p_0)$ and

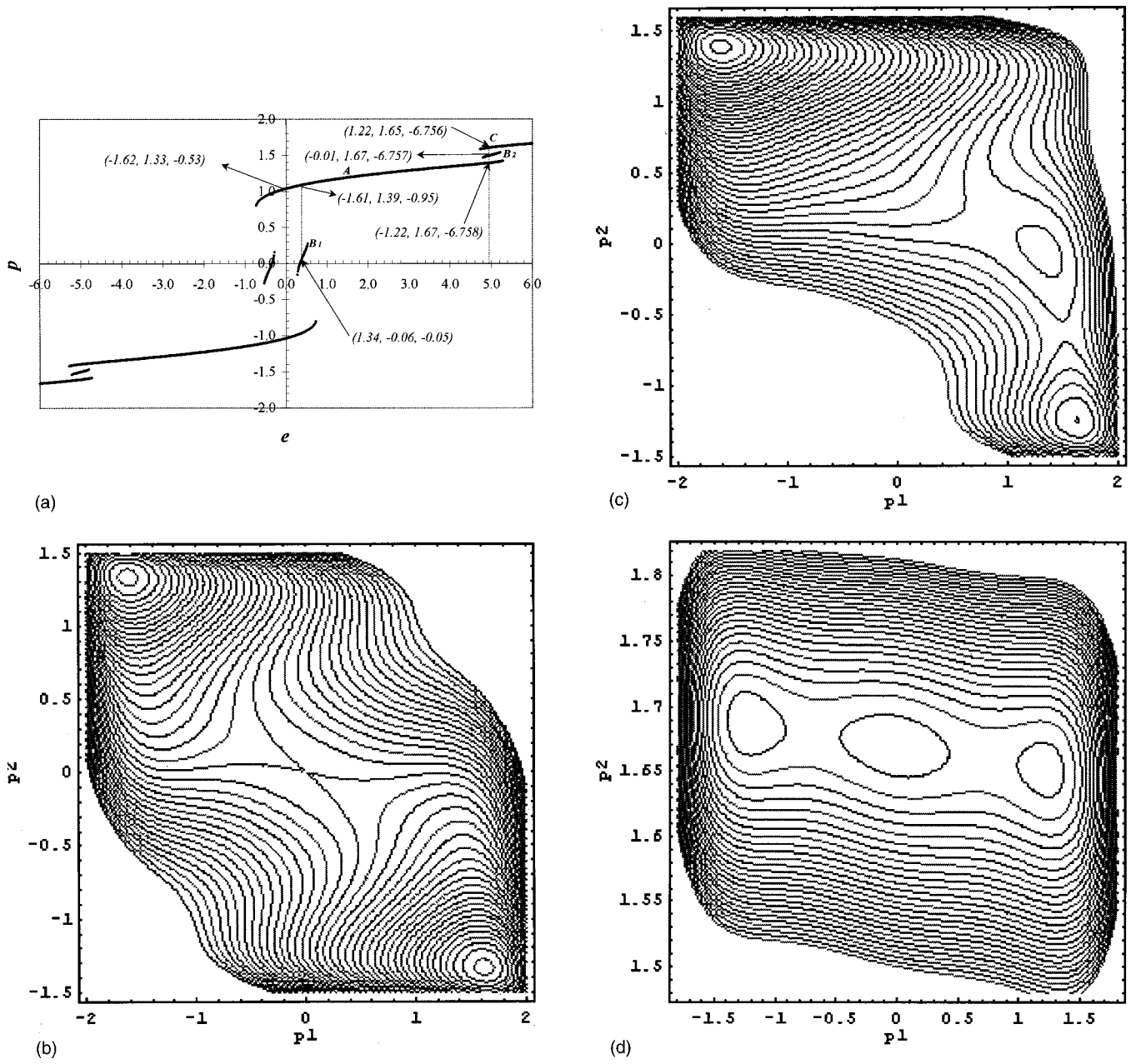

FIG. 6. (a) Calculated DHL's for $j=0.3$, $l=0.1$, and $t=0.8$ ($t<t_{SC}$). Contour plots are shown for (b) $e=0$, (c) $e=0.4$, and (d) $e=5.0$. The annotations shown in (a), in the form (p_1,p_2,f), are the locations of minima of f and values of f at minima. These minima correspond to the minimum points in the contour plots in (b)–(d).

$(-p_0,p_0)$ relative to the two in which p_1 and p_2 have the same sign. In addition, as remarked in Sec. II, f_C destabilizes the PE phase, as seen in the value $t_{SC}=2j>0$ in Eq. (17). Finally, the field term f_E favors an alignment of both p_1 and p_2 in the direction of e, and obviously this becomes the dominant term for large e.

We now show some examples of the DHL for some typical parameter values. In addition to numerical solution of Eqs. (9) and (10), with subsequent evaluation of f from Eq. (15) where necessary, we applied algebraic software (MATHEMATICA) to make three-dimensional and contour plots of f versus p_1 and p_2. We find that the form of the DHL depends mainly on where the temperature t is located relative to the critical temperatures in Eq. (17), and we start by discussing the DHL mainly for the coupling value $j=0.3$ at various temperatures. For $j=0.3$, obviously, $t_{SC}=0.6$, $t_C=1.35$, $t_{SH}=1.6$, and $t_2=2.4$.

The DHL for a temperature below t_{SC} is shown in Fig. 1(a). There are three branches as labeled. For $e=0$ the PE phase is not stable and point A, corresponds to the AF phase $(p_0,-p_0)$. The value of j is sufficiently small that there is a second local minimum at C; this is a shifted form of the point (p_0,p_0) that was noted as an equivalent minimum for $j=0$. A contour plot of the f surface for $e=0$ is shown in Fig. 1(b). As seen there, and as noted in the annotations in Fig. 1(a), the C minima are much shallower than the A

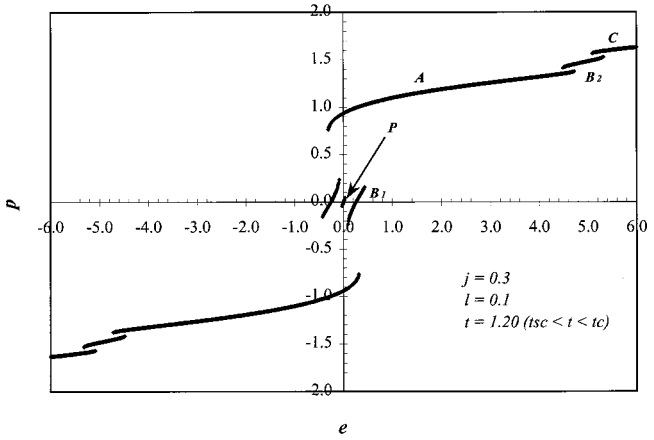

FIG. 7. Calculated DHL's for $j=0.3$, $l=0.1$, and $t=1.2$ $(t_{SC}<t<t_C)$.

minima. As j increases, the C minimum for $e=0$ becomes shallower and vanishes for sufficiently large j.

As seen in Fig. 1(a), the A line persists to some value e_{CA} of e above which it disappears and only the C line is stable. An additional section B is seen for a small range of intermediate field values. A contour plot for $e=0.9$ is shown in Fig. 1(c) with the minima identified with the annotations in Fig. 1(a). Like all graphs for nonzero e, the contour plot has reflection symmetry about the line $p_1=p_2$. The graph and the figure show that B corresponds to a minimum point with p_1 large and $p_2\approx 0$, or vice versa.

The qualitative form of the DHL shown in Fig. 1(a) persists up to $t=t_{SC}$ with qualitative changes as follows for increasing t. First, the C line eventually does not cross the $e=0$ axis, but appears only at a nonzero value of e. Second, e_{CA} decreases; the A line becomes shorter. Third, the B line becomes longer. We remark that the converse is true: with decreasing t the B line becomes shorter and eventually disappears.

Some indication of the effect of changing j is given by Fig. 1(d). As commented upon above, for this larger j, the C minimum at $e=0$ is absent, with the C line starting only at non-zero e. In addition, the B line is absent. Since at a B point $p_1p_2\approx 0$ larger j disfavors B compared with A for which p_1p_2 is negative and of some magnitude. The form of the DHL in Fig. 1(d) is similar to that found in second-order antiferroelectrics.

Figure 2(a), again for $j=0.3$, shows the DHL for a temperature in the range $t_{SC}<t<t_C$; the qualitative form is similar for the whole interval $t_{SC}<t<t_{SH}$ in which both the PE and antiferromagnetic (AF) phases are locally stable. The main difference from Fig. 1(a) is the appearance of a second line, labeled P, in the low-field region. The contour plot for $e=0.2$, [Fig. 2(b)], and the annotations in Fig. 2(a) show that this line corresponds to the PE phase (small and equal field-induced values of p_1 and p_2). For higher field values curves A, B, and C are identified in Fig. 2(a). The contour plot for $e=0.7$, Fig. 2(c), and the annotations in Fig. 2(a) show that these have the same character as the corresponding curves in Fig. 1(a).

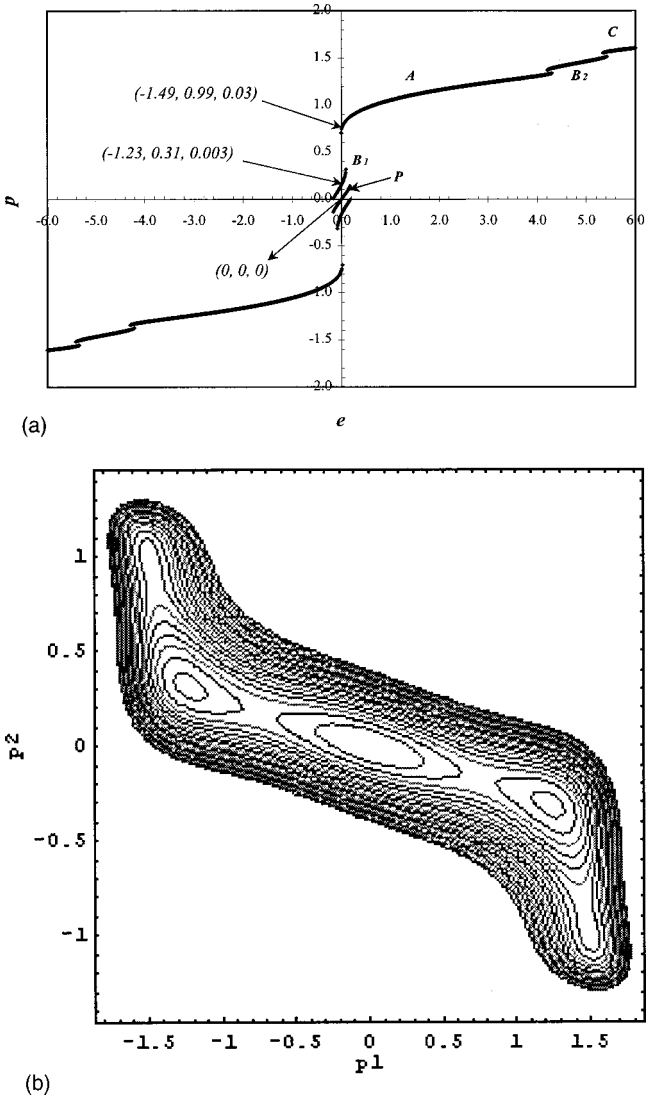

FIG. 8. (a) Calculated DHL's for $j=0.3$, $l=0.1$, and $t=1.5$ $(t_C<t<t_{SH})$. (b) Contour plot for $e=0$ with relevant annotations shown in (a).

As t increases toward t_{SH}, the AF phase becomes relatively less stable and, on the DHL the A line becomes shorter and the P line longer. Above t_{SH} the AF phase is not locally stable for $e=0$, and consequently the A line no longer appears, as illustrated in Fig. 3. Otherwise, as seen, the DHL retains the same general form with P, B, and C portions. Table I gives a summary on the behavior of lines in the DHL for $l=0.5$ and $j=0.3$, with temperature t. These lines show a similar behavior in the DHL for $j=0.3$ and 0.5. A distinct quadruple-loop DHL is seen in the temperature range of $t_{SH}<t<t_2$.

We remarked that a biquadratic interface coupling term $F_{BQ}=J_2P_1^2P_2^2$ in the free energy is allowable by symmetry. We have not carried out detailed studies of the effects that might be due to such a term but it is not difficult to make some qualitative comments. For positive J_2, the surface describing F_{BQ} as a function of P_1 and P_2 is as follows. Along either axis, F_{BQ} is zero. At a given radius from the origin, F_{BQ} attains its maximum value along the 45° lines $P_1=$

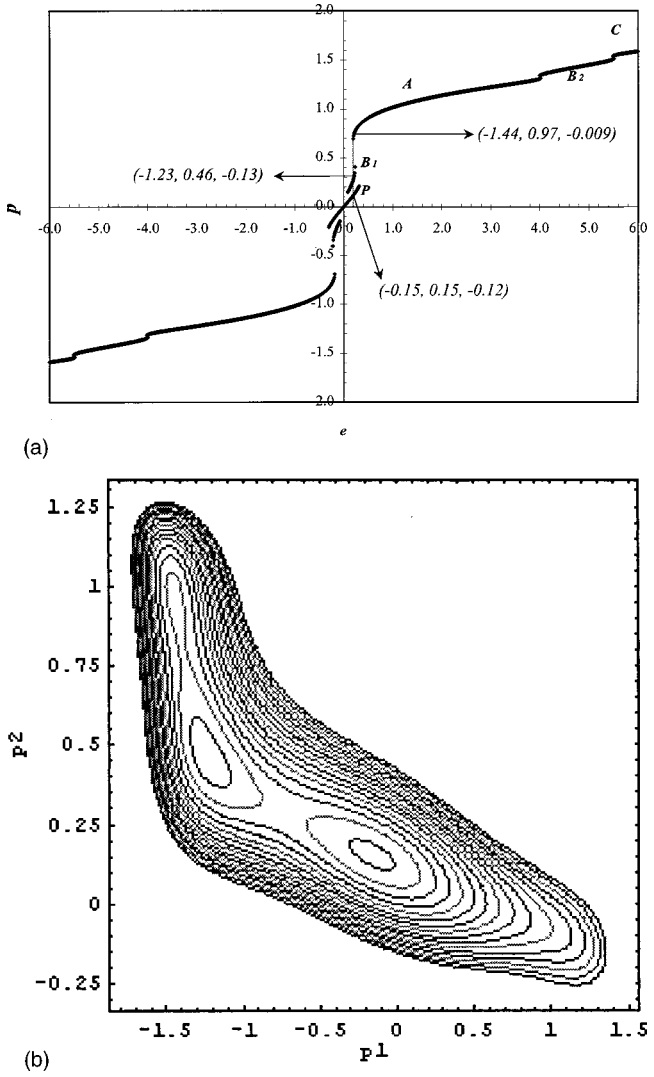

FIG. 9. (a) Calculated DHL for $j=0.3$, $l=0.1$, and $t=1.7$ ($t>t_{SH}$). (b) Contour plot for $e=0.2$ with relevant annotations shown in (a).

$\pm P_2$, and increases strongly with distance from the origin. Thus the addition of F_{BQ} into the free energy favors states with P_1 or P_2 near zero, as on lines *B* or *P* (the PE phase), and disfavors the AF and FE states, lines *A* and *C*. In Fig. 2(a), for example, one would expect the *e*-axis lengths of lines *A* (AF) and *C* (FE) to decrease, and the lengths of *P* and *B* to increase.

IV. GENERAL THICKNESS RATIO

For general *l*, we may expect that, as in the second-order case,[6] the properties of the bilayer are intermediate between those of a ferroelectric for $l\approx 0$ and 1 and an antiferroelectric for $l\approx 0.5$. To some extent the form of the hysteresis loop depends on the whereabouts of the temperature with respect to the critical values t_{SC}, etc., so we start by showing (in Fig. 4) the variation of these with *j* and *l*. Since, obviously, the values for $1-l$ are the same as those for *l*, the *l* axis runs from 0 to 0.5. The first temperature, t_{SC}, is calculated from the analytical formula [Eq. (13)], while t_C and t_{SH} are found numerically: t_C is the temperature at which the free energies of local minima representing the paraelectric phase and an ordered phase with $(p_1,p_2)\neq 0$ are equal, and t_{SH} is the highest temperature to which an ordered phase persists. According to Eq. (13), and as seen in Fig. 4(a) t_{SC} diverges as $l\to 0$ or $l\to 1$ and takes its minimum value for $l=0.5$; it is seen from Figs. 4(b) and 4(c) that the same holds for t_C and t_{SH}.

For illustration, we take $j=0.3$ and two values of *l*, 0.1 and 0.3, so that we are looking at the extension of results like Figs. 1–3 to unequal thickness. For $e=0$ the ordered state with p_1 and p_2 nonzero generally corresponds to a nonzero polarization $p=lp_1+(1-l)p_2$ and it is helpful to start with the temperature variation of *p* in zero field, as shown in Fig. 5. The paraelectric phase $p=0$, which runs from $t=t_{SC}$ upward, is not shown explicitly. For the higher value of *l* [Fig. 5(b)], the graph is similar to that for a bulk first-order material with supercooling and superheating temperatures as marked and an equilibrium phase transition at t_C where $f=0$. Figure 5(a) is more complicated, with two separate ordered phases marked as *U* and *L*. As seen in the inset graph, the corresponding free energies become equal, $f_U=f_L$ at a temperature t_{C1}, and $f_L=0$ at t_{C2}. Thus two phase transitions occur. A previous prediction of two phase transitions in a first-order ferroelectric system was given by Scott *et al.*[10] They were concerned with a single film in which the Landau-Devonshire theory was extended to allow for spatial variation of *p*, and they found that in some cases there were two transitions, the lower one from a ''bulklike'' ordered phase to a ''surfacelike'' one, and the upper from the surfacelike phase to the paraelectric phase.

We now turn to calculated DHLs, starting with $l=0.1$. Figure 6 shows an example of a low-temperature DHL, with some relevant contour plots. The contour plot in Fig. 6(b) and the annotations in Fig. 6(a) confirm that, as expected, the states at $e=0$ have values of p_1 and p_2 that are large in magnitude and opposite in sign. They are antiferroelectric, or more accurately ferrielectric, in character, and in accordance with Figs. 1 and 2 we label them *A*. For $e=0.4$, Fig. 6(c) and the annotations in Fig. 6(a) show the two *A* points, with opposite signs of p_1 and p_2, and they identify the short intermediate line as a *B* type line with p_1 large and p_2 near zero. We mark it as B_1. Figure 6(d) and the annotations in Fig. 6(a) correspond to the triple-valued region at high field. They confirm that curve *A* is still antiferroelectric in character, with p_1 negative and p_2 positive. The persistence of this state to a high-field value is explained by the small value of *l*. The dominant term in the free energy is the field coupling to p_2 so that p_2 is positive (as it is at all three local minima) and the exchange coupling then drives p_1 negative. The intermediate curve is identified as *B* type, now with p_2 large and p_1 near zero; we denote it B_2. The high-*p* curve *C* is the fully aligned state with both p_1 and p_2 positive; it obviously persists to higher fields. Thus, as seen in Fig. 6(d), the three local minima all have p_2 positive because of the large field

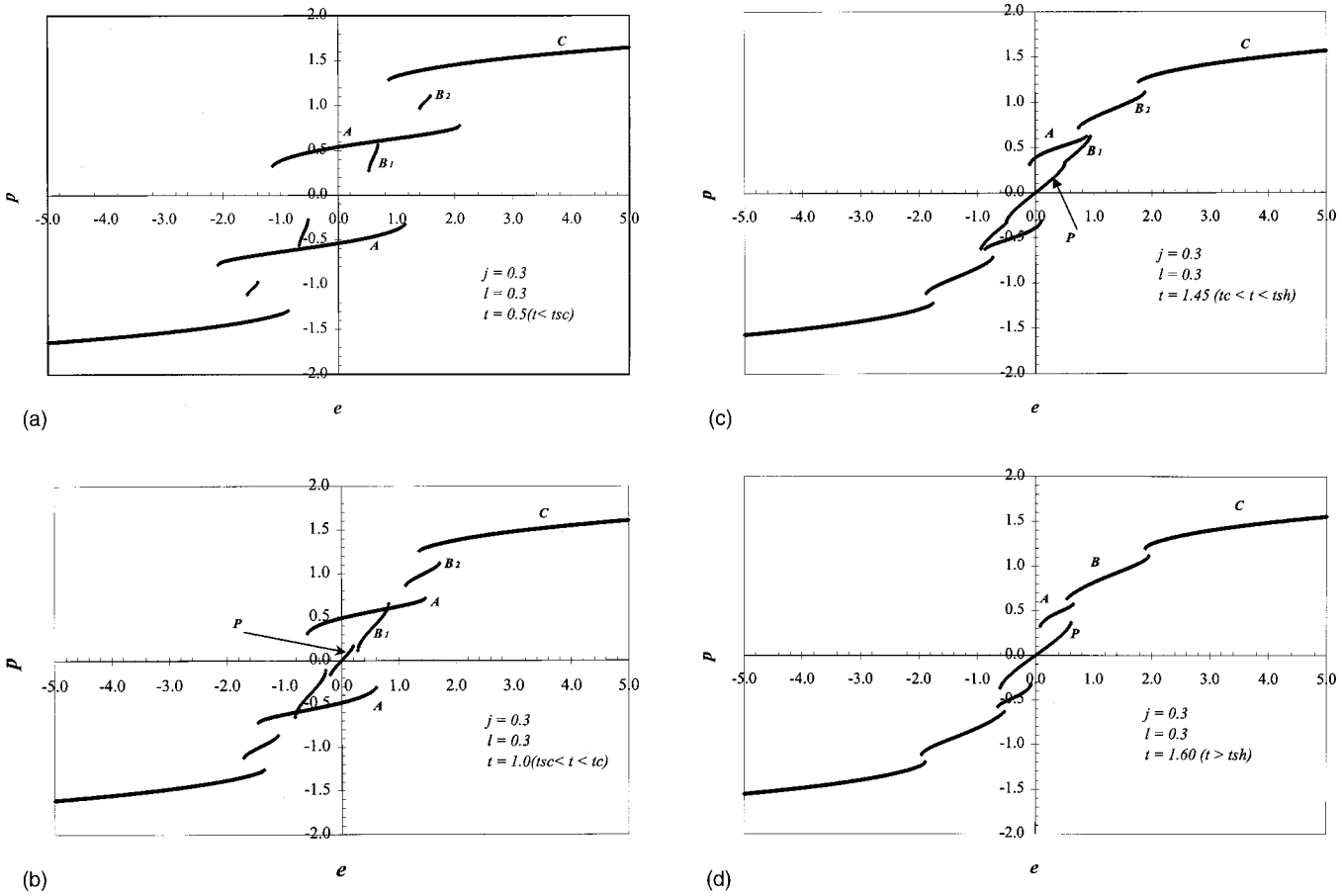

FIG. 10. Calculated DHL's for $j=0.3$ and $l=0.3$. (a) $t=0.5$, $t<t_{SC}$. (b) $t=1.0$, $t_{SC}<t<t_C$. (c) $t=1.45$, $t_C<t<t_{SH}$. (d) $t=1.6$, $t>t_{SH}$.

energy, while p_1 is successively negative, near zero, and positive.

Figure 7 is the DHL for $l=0.1$ and $t=1.2$, in the interval $t_{SC}<t<t_C$. Since the paraelectric phase is now locally stable a line, marked *P*, appears in the low-field region. We have confirmed from a contour plot that this is indeed the paraelectric phase, with p_1 and p_2 both near zero. The rest of the DHL contains lines B_1, *A*, B_2, and *C* which are similar in character to those in Fig. 6(a).

Figure 8(a) is the DHL for $l=0.1$ and $t=1.5$, in the interval $t_C<t<t_{SH}$. As seen from Fig. 5(a), this is in the temperature range where there are two locally stable ordered phases in addition to the paraelectric phase. The nature of the phases at $e=0$ is clarified by the contour plot in Fig. 8(b) and the annotations in Fig. 8(a). The larger value of *p* has an ''antiferroelectric'' character, with p_1 and p_2 opposite in sign and relatively large. The smaller *p* corresponds to a smaller value of p_2. We label this part of the DHL as B_1, since it evolves from the corresponding portion of Fig. 7. The other parts have the same identification as in previous figures.

Finally for this value of *l* we show in Fig. 9(a) the DHL for $t=1.7$, for which $t>t_{SH}$. Lines *P*, B_1, *A*, B_2, and *C* are identified as in previous figures. As seen from the contour plot in Fig. 9(b) and the values in the annotations in Fig. 9(a), the B_1 point is quite well away from the line $p_1=0$, but the other lines have the same character as discussed previously.

Figure 10 shows calculated DHL's for the various temperature ranges for the larger value $l=0.3$; these are naturally intermediate in character between those for $l=0.1$ and 0.5. The main qualitative differences between these curves and those for $l=0.1$ are due to the fact that since side 1 is thicker, the field coupling to p_1 is stronger so that it energetically less favorable for p_1 to be in the opposite direction to *e*. Consequently the *A* lines are shorter, and the final switch to the *C* line, on which both p_1 and p_2 are aligned along *e*, takes place at a lower field value. Converse statements describe the comparison with the DHL's for $l=0.5$. Another noteworthy feature of Fig. 10 is that although a B_1 line is present, except in Fig. 10(d), it never crosses the $e=0$ axis, in agreement with Fig. 5(b).

In order to have a clearer picture on the variation of the lines in the DHL, which is more varied, a summary on the behavior of the lines in the DHL for a few temperature ranges is given in Table II for $l=0.1$. Many similarities in the behavior of lines in the DHL between cases of $l=0.1$ and 0.3 are observed. Hence, another table for $l=0.3$ is not necessary. We wish to point out that B_1 line disappears, within the temperature range of $t_{SH}<t<t_2$, in $l=0.3$ first then in $l=0.1$ as can be seen in Fig. 10(d). The six-loop-DHL can

TABLE II. Summary of the behavior of lines in the DHL for $l=0.1$ and $j=0.3$ with t.

t	A line	B line	C line	P line
$t<t_{SC}$	Splits into upper and lower lines, becomes shorter as t increases	B_1 and B_2 lines appear as t increases, for $e\neq 0$	Appears for $e\neq 0$	Does not appear
$t_{SC}<t<t_C$	Splits into upper and lower lines, becomes shorter as t increases	B_1 draws nearer to (0, 0) and shifts downward and B_2 becomes longer	Appears for $e\neq 0$	Begins to appear
$t_C<t<t_{SH}$	Splits into upper and lower lines, becomes shorter as t increases	B_1 draws nearer to (0, 0) and shifts downward and B_2 becomes longer	Appears at higher e	Becomes longer
$t_{SH}<t<t_2$	Splits into upper and lower lines, becomes shorter as t increases	B_1 line disappears only when t is closer to t_2. B_2 becomes longer	Appears at even higher e	Becomes longer

only appear as soon as the B_1 line disappears within the upper temperature range mentioned.

V. CONCLUSIONS

Here we have presented a generalization of our previous account[6] of bilayers to the practically important case of first-order materials. Although we have not stressed the point, the calculations apply equally to two-component superlattices, as mentioned previously.[6] For the special case of equal layer thicknesses, our free energy expression is the same as that for a bulk first-order antiferroelectric. As far as we are aware, there is no detailed account of the DHL for this in the literature so we have discussed it in Sec. III. In addition to the expected A phase, in which p_1 and p_2 are both large and of opposite sign, the paraelectric P phase in which both are small and the high-field C phase in which both p_1 and p_2 are aligned along the field, we have found that in some field and temperature intervals there is a B phase in which one of p_1 and p_2 is large and the other is near zero. This leads to some intermediate segments on the calculated DHL's.

For unequal layer thicknesses our system might be called an engineered ferroelectric. At first sight the DHL's appear quite complex, but we have found that a simple classification into P, A, B_1, B_2, and C segments works surprisingly well in understanding the field regions occupied by the various segments. We should draw attention to the two thermodynamic phase transition temperatures identified in Fig. 5(a), and explored further in Figs. 8(a) and 8(b). We should also make the obvious comment that we have considered only the special case when the component materials of the bilayer are the same, since this enabled us to concentrate on the effects of the coupling term. The DHL's for more general systems might not answer to such a simple classification scheme as we have used here.

All the features discussed above involving the B and P lines are not present in the DHL of Ref. 6, because the temperature t in a second-order phase transition does not play a crucial role in establishing features of the hysteresis loop. In Ref. 6 we commented on the implications of our results for the design of bilayers or superlattices with specified hysteresis loops. As we have seen, the form of the DHL is sensitive to the value of the dimensionless coupling constant j. However, as seen in Eq. (8), j is proportional to $J/(L_1+L_2)$, where J is the interface coupling in (1) and L_1+L_2 is the total thickness. Thus the value of j can be selected by design of L_1+L_2. The other main parameter affecting the hysteresis loops is the dimensionless thickness ratio $l=L_1/(L_1+L_2)$, and obviously this can be selected too. As we have seen, the extra complexity of first-order materials compared with second-order introduces further flexibility.

[1] S. Ducharme, V. M. Fridkin, A. V. Bune, S. P. Palto, L. M. Blinov, N. N. Pethukova, and S. G. Yudin, Phys. Rev. Lett. **84**, 175 (2000).

[2] D. Ricinschi, C. Harnagae, C. Ppusoi, L. Mitoseriut, V. Tora, and M. Oyukawa, J. Phys.: Condens. Matter **10**, 477 (1998).

[3] M. E. Lines and A. M. Glass, *Principles and Applications of Ferroelectrics and Related Materials* (Clarendon, London, 1977).

[4] W. L. Zhong, *The Physics of Ferroelectrics* (Science, Beijing, 1998).

[5] W. Kanzig, *Ferroelectrics and Antiferroelectrics* (Academic, New York, 1957).

[6] K.-H. Chew, L.-H. Ong, Junaidah Osman, and D. R. Tilley, Appl. Phys. Lett. **77**, 2755 (2000).

[7] A. Fert, P. Grunberg, A. Barthelemy, F. Tefroff, and W. Zinn, J. Magn. Magn. Mater. **140–144**, 1 (1995).

[8] B. D. Qu, W. L. Zhong, and R. H. Prince, Phys. Rev. B **55**, 11 218 (1997).

[9] E.-K. Tan, Junaidah Osman and D. R. Tilley, Solid State Commun. **116**, 61 (2000).

[10] J. F. Scott, H. M. Duiker, P. D. Beale, B. Pouligny, K. Dimmler, M. Parris, D. Butler, and S. Eaton, Physica B **150**, 160 (1988).